Progressive Freezing of Composites Analyzed by Isotherm Migration Methods

YESHAYAHU TALMON,
H. T. DAVIS
and
L. E. SCRIVEN

Department of Chemical Engineering and Materials Science
University of Minnesota
Minneapolis, MN 55455

The Isotherm Migration Method of numerically analyzing conduction with phase change is modified to handle surface and external resistances, appearance, and propagation of successive fronts into slabs of composite material of one or more constituents finely dispersed in a matrix, different components transforming at different temperatures. Procedures are developed for selecting temperature intervals between isotherms, initially locating isotherms by means of analytical approximations to the earliest stages, and thereafter inserting and removing isotherms as appropriate, particularly when each component gives rise to a separate front.

SCOPE

The propagation of phase boundaries under circumstances of heating or cooling is an important subset of Stefan problems. Thermally driven phase boundaries are encountered in many practical situations, examples being manufacturing processes based on solidification, casting and molding; food processes such as freezing, thawing, drying and cooking; solid-solid phase transitions including electrical and magnetic changes; and weather-related phenomena such as freezing and thawing of soil and of bodies of surface water.

Although analytical solutions are known for a few moving boundary problems, most can be handled only by numerical methods. A technique especially convenient for one-dimensional problems involving phase boundaries, or transformation fronts of fixed temperature, is the Isotherm Migration Method (IMM), which was proposed by Dix and Cizek (1971) and by Chernous'ko (1970). In the IMM, temperature is replaced by distance as the dependent variable. Thus one tracks in time t the position x of a given isotherm u. Crank and Phahle (1973) developed a finite difference solution of the one-dimensional isotherm migration problem associated with the melting of an ice slab initially at its freezing point and suddenly subjected to a fixed thawing temperature at its surfaces. Crank and Gupta (1975) extended the IMM to the solution of a two-dimensional problem.

The problem treated by Crank and Phahle, although it demonstrates the simplicity and accuracy of their method, is of rather limited applicability. In many important cases the heated or cooled material is a multiphase composite in which several fronts can propagate simultaneously. Moreover, the temperature of a contacting fluid is more often controlled, rather than the temperature of the sample surface. As pointed out by Shamsundar (1978), the IMM is faced with difficulties when it is applied to situations where the boundary temperatures are unknown as, for example, in the case of a radiation-type boundary condition (also known as a mixed boundary condition and as a boundary condition of the third kind).

The purpose of this paper is to develop and apply a flexible numerical method for solving one-dimensional Stefan problems in which there is more than one moving front and the condition at the exposed surface is of radiation type. Although examples illustrated are for constant transfer coefficients, the numerical methods developed are applicable to variable coefficients as well.

CONCLUSIONS AND SIGNIFICANCE

The Isotherm Migration Method (IMM) as used by Crank and his coworkers (1973, 1975) is extended to solve problems which involve several moving boundaries of change of phase, such as the freezing or melting of composite slabs. IMM is restricted to slabs with a fixed surface temperature. In addition to extending IMM we have developed the Modified Isotherm Migration Method (MIMM) which can handle problems with surface and external resistances. In our version of the IMM one starts with all isotherms present in the slab, and removes them as they reach the midplane. In the MIMM a mechanism is provided for the addition and for the removal of isotherms with the propagation of the solution, as the surface and the midplane temperatures change with time.

The applicability of the IMM and the MIMM is demonstrated by calculations of freezing of thin films (200 nm) and slabs (0.02 m) of water and of tetradecane-in-water dispersions immersed in a cryogenic coolant. In these examples we show that the numerical methods we developed can also be used to uncover ranges of conditions and parameters in which simple approximations can be used instead of the detailed numerical solution, thus reducing the effort and computational cost.

Y. Talmon is presently with the Department of Chemical Engineering, Technion-Israel Institute of Technology, Haifa, Israel 32000.

0001-1541-81-4963-0928-$2.00.

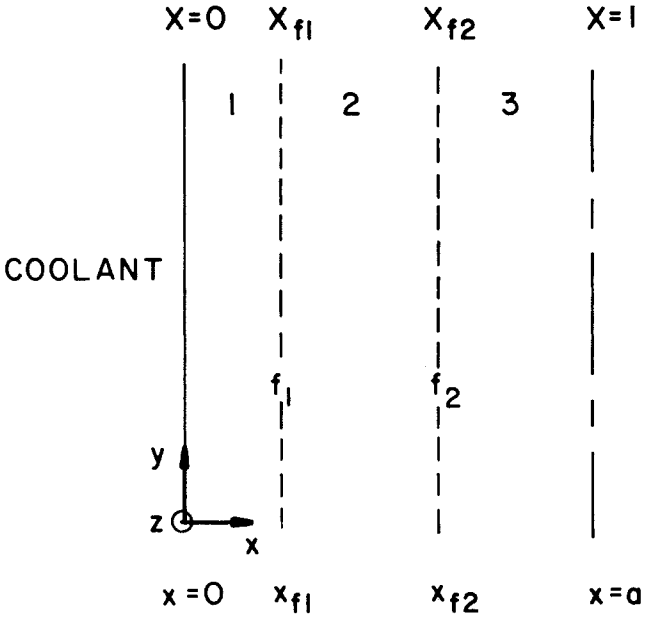

Figure 1. Idealized model of the slab. Only the left-hand half is shown; $x = a$ is the plane of symmetry. The two moving fronts f_1 and f_2 define three regions: 1, solid-solid; 2, solid-liquid; and 3, liquid-liquid.

THE PHYSICAL MODEL

Figure 1 illustrates the freezing slab to be studied. The slab is symmetric about $x = a$ and it contains a fine dispersion of one liquid in another. At $t = 0$ the slab is suddenly immersed in a coolant. As it cools, the liquid with the higher freezing point will start freezing first. As the slab is further cooled the freezing front will advance towards the midplane, leaving behind a dispersion of solid in liquid or liquid in solid. Meanwhile, when the surface temperature passes the freezing point of the second liquid, a second freezing front will form and start advancing in the x-direction, leaving behind completely frozen material. Both liquids in the neighborhood of the plane at any given distance x are presumed to have the same temperature. Three regions are formed in the sample: region 1, solid-solid; region 2, solid-liquid; region 3, liquid-liquid. The first front, f_1, separates regions 1 and 2 and the second front, f_2, separates regions 2 and 3. Eventually f_2 and its mirror image will reach the mid-plane leaving only regions 1 and 2 in the sample. When f_1 and its mirror image get there, the solidification of the sample is finished.

In our model each region has its own thermal properties which are set by its composition and are taken to be temperature-independent. Any change of density with change of phase is neglected. The structure of the slab can be maintained by an internal solid network within which the fluids are interspersed or by solid films at the outer surfaces. In the latter case our analysis holds insofar as the heat transfer through the confining films can be modelled with a heat transfer coefficient (i.e., the quasi-steady-state approximation within the outer films holds).

THE MATHEMATICAL MODEL

We denote the single local temperature in each of the three regions as u_1, u_2, and u_3. We assume throughout the paper that physical parameters are constant. The thermal diffusivity of the i-th region is κ_i and its thermal conductivity is K_i. The positions of the two freezing fronts are x_{f1} and x_{f2}. Within each region the temperature must satisfy the heat conduction equation:

$$\frac{\partial^2 u_i}{\partial x^2} - \frac{1}{\kappa_i}\frac{\partial u_i}{\partial t} = 0 \tag{1}$$

When the front x_{fi} moves a distance dx_{fi}, a quantity of heat $L_i\rho_i dx_{fi}$ is liberated and must be removed by conduction, thus for the two moving fronts we have:

$$K_i \frac{\partial u_i}{\partial x} - K_{i+1}\frac{\partial u_{i+1}}{\partial x} = L_i\rho_i \frac{dx_{fi}}{dt}, \quad x = x_{fi} \tag{2}$$

$L_i \equiv \phi_i l_i$, where l_i is the latent heat of the component which undergoes phase change at x_{fi}, ϕ_i is its volume fraction in the system, and ρ_i is the density of region i. In addition we have continuity of temperature at the two fronts,

$$u_i(x_{fi}, t) = u_{i+1}(x_{fi}, t) = u_{fi}, \tag{3}$$

and from the symmetry of the problem,

$$\left.\frac{\partial u_m}{\partial x}\right|_{x=a} = 0, \tag{4}$$

where m refers to whichever region is nearest to $x = a$. We have also the initial condition

$$u(x, 0) = u_o, \tag{5}$$

where u_o is not necessarily the freezing point of one of the components of the dispersion.

To complete the definition of the problem, the thermal resistance of the fluid coolant and any confining films must be specified. In what follows we solve the problem with the so-called "third kind" or "radiation boundary" condition,

$$h[u_j(0, t) - u_a] = K_j \left.\frac{\partial u_j}{\partial x}\right|_{x=0}, \tag{6}$$

where h is the heat transfer coefficient of coolant and film, j refers to the region adjacent to $x = 0$, and u_a is the coolant bulk temperature. The limit as $h \to \infty$ corresponds to the boundary condition

$$u_j(0, t) = u_a \tag{7}$$

and is included in our analysis.

In terms of the variables $X \equiv x/a$, $T \equiv \kappa_1 t/a^2$, $S_1 \equiv \rho L_1\kappa_1/K_1$, $S_2 \equiv \rho L_2\kappa_1/K_2$, $\alpha \equiv \kappa_2/\kappa_1$, $\beta \equiv K_2/K_1$, $\gamma \equiv k_3/k_1$, $\delta \equiv K_3/K_2$, Eq. 1 becomes:

$$\frac{\partial u_1}{\partial T} = \frac{\partial^2 u_1}{\partial X^2}, \quad 0 < X < X_{f1} \tag{8}$$

$$\frac{\partial u_2}{\partial T} = \alpha\frac{\partial^2 u_2}{\partial X^2}, \quad X_{f1} < X < X_{f2} \tag{9}$$

$$\frac{\partial u_3}{\partial T} = \gamma\frac{\partial^2 u_3}{\partial X^2}, \quad X_{f2} < X < 1 \tag{10}$$

Equation 2 becomes:

$$\frac{\partial u_1}{\partial X} - \beta\frac{\partial u_2}{\partial X} = S_1\frac{dX_{f1}}{dT}, \quad X = X_{f1} \tag{11}$$

$$\frac{\partial u_2}{\partial X} - \delta\frac{\partial u_3}{\partial X} = S_2\frac{dX_{f2}}{dT}, \quad X = X_{f2} \tag{12}$$

Boundary condition (Eq. 6) becomes

$$ha[u_j(0, T) - u_a] = K_j \left.\frac{\partial u_j}{\partial X}\right|_{X=0} \tag{13}$$

and the new forms of Eqs. 3-5 and of Eq. 7 are obvious.

When the problem involves freezing of just one phase we have only two of the Eqs. 8-10 and only one equation of Eqs. 11-12. It should be noted that any number of phase transitions can be taken into account by defining new regions and adding the appropriate equations. The formulation is not limited to freezing problems: it can be applied to any kind of phase change involving moving boundaries.

THE ISOTHERM MIGRATION METHOD (IMM)

Whereas the temperature, u, customarily is expressed as a function of the independent variable, X, and time, T, i.e., $u =$

$u(X, T)$, in the IMM X is expressed as a function of u and T: we calculate the position $X = X(u, T)$ of a given isotherm at a known time. Although convenient for solving Stefan-type problems, the IMM poses several restrictions that must be considered carefully. We must start with all the isotherms that are used in the calculation already in the interval $0 < X < 1$. As a result the IMM can be used only with the boundary condition (Eq. 7). We also need an initial temperature profile to locate these isotherms before we start the numerical procedure. Thereafter when any isotherm reaches the midplane it must be discarded. Moreover, as it approaches $X = 1$ it must be advanced in such a way that the symmetry condition at $X = 1$ is satisfied.

To use the IMM we rewrite Eqs. 8-13 so that X is expressed as a function of u and T. Since

$$\frac{\partial u}{\partial X} = \left(\frac{\partial X}{\partial u}\right)^{-1} \quad \text{and} \quad \left(\frac{\partial X}{\partial T}\right)_u = -\left(\frac{\partial u}{\partial T}\right)_X \left(\frac{\partial X}{\partial u}\right)_T \tag{14}$$

we have:

$$\frac{\partial X}{\partial T} = \left(\frac{\partial X}{\partial u_1}\right)^{-2}\left(\frac{\partial^2 X}{\partial^2 u_1}\right) \quad 0 < X < X_{f1} \tag{15}$$

$$\frac{\partial X}{\partial T} = \alpha\left(\frac{\partial X}{\partial u_2}\right)^{-2}\left(\frac{\partial^2 X}{\partial^2 u_2}\right) \quad X_{f1} < X < X_{f2} \tag{16}$$

$$\frac{\partial X}{\partial T} = \gamma\left(\frac{\partial X}{\partial u_3}\right)^{-2}\left(\frac{\partial^2 X}{\partial^2 u_3}\right) \quad X_{f2} < X < 1 \tag{17}$$

$$S_1 \frac{dX_{f1}}{dT} = \left(\frac{\partial X}{\partial u_1}\right)^{-1} - \beta\left(\frac{\partial X}{\partial u_2}\right)^{-1} \quad X = X_{f1} \tag{18}$$

$$S_2 \frac{dX_{f2}}{dT} = \left(\frac{\partial X}{\partial u_2}\right)^{-1} - \delta\left(\frac{\partial X}{\partial u_3}\right)^{-1} \quad X = X_{f2} \tag{19}$$

The boundary and initial conditions take the form:

$$X = X_{f1} \quad \text{at} \quad u = u_{f1} \tag{20}$$

$$X = X_{f2} \quad \text{at} \quad u = u_{f2} \tag{21}$$

and from Eq. 7,

$$X = 0 \quad \text{at } u = u_a. \tag{22}$$

The symmetry condition and Eq. 13 are used in their original form in the numerical procedure. As the solution proceeds u_{f2} eventually reaches $X = 1$; then region 3 disappears from the slab and Eqs. 17, 19 and 21 are not used anymore.

The derivatives in Eqs. 15-19 are approximated by three-point centered finite differences, which give X of the i-th isotherm after $n + 1$ time steps in terms of values already known from the time-step. If Δu_j is the temperature difference between the isotherms in region j and ΔT^n is the dimensionless time difference between the n-th and the $n + 1$-st steps, we get from Eqs. 15-17

$$X_i^{n+1} = X_i^n + 4\Delta T^n\left[\frac{X_{i+1}^n - 2X_i^n + X_{i-1}^n}{(X_{i-1}^n - X_{i+1}^n)^2}\right], \quad \text{region 1} \tag{23}$$

$$X_i^{n+1} = X_i^n + 4\alpha\Delta T^n\left[\frac{X_{i+1}^n - 2X_i^n + X_{i-1}^n}{(X_{i-1}^n - X_{i+1}^n)^2}\right], \quad \text{region 2} \tag{24}$$

$$X_i^{n+1} = X_i^n + 4\gamma\Delta T^n\left[\frac{X_{i+1}^n - 2X_i^n + X_{i-1}^n}{(X_{i-1}^n - X_{i+1}^n)^2}\right], \quad \text{region 3} \tag{25}$$

and from Eqs. 18-19

$$X_{f1}^{n+1} = X_{f1}^n + \frac{\Delta T^n}{S_1}\left[\frac{\Delta u_1}{X_{f1} - X_{f1-1}} - \frac{\beta\Delta u_2}{X_{f1+1}^n - X_{f1}^n}\right] \tag{26}$$

$$X_{f2}^{n+1} = X_{f2}^n + \frac{\Delta T^n}{S_2}\left[\frac{\Delta u_2}{X_{f2} - X_{f2-1}} - \frac{\delta\Delta u_3}{X_{f2+1}^n - X_{f2}^n}\right] \tag{27}$$

X_{fj-1} denotes the position of the first isotherm to the left (smaller X) of X_{fj}, and X_{fj+1} denotes the position of the first isotherm to the right of X_{fj}.

Rigorous stability analysis for the IMM is not available. Dix and Cizek (1971) considered instead the coefficient of X_i^n in Eqs. 23-25. This coefficient must be positive for X_i^{n+1} to increase with an increase in X_i^n. This conservative requirement leads to the criteria

$$\Delta T^n < \frac{1}{8}(X_{i+1}^n - X_{i-1}^n)^2 \quad \text{in region 1} \tag{28}$$

$$\Delta T^n < \frac{1}{8\alpha}(X_{i+1}^n - X_{i-1}^n)^2 \quad \text{in region 2} \tag{29}$$

$$\Delta T^n < \frac{1}{8\gamma}(X_{i+1}^n - X_{i-1}^n)^2 \quad \text{in region 3} \tag{30}$$

In practice, after each step ΔT^n is calculated for all isotherm pairs according to Eqs. 28-30 and the smallest one is chosen as ΔT for the next iteration. The truncation error of the IMM is proportional to ΔT and to $(\Delta u)^2$ (Dix and Cizek, 1971).

To start the solution an initial temperature profile is needed. In some cases this can be calculated from analytic solutions for semi-infinite regions (Carslaw and Jaeger, 1959; Schneider, 1955).

The method of solution just described is an extension of that used by Crank and Phahle (1973) to solve the relatively simple case of melting ice initially at its freezing point. In that case the region between the moving front and $X = 1$ remains at 0°C and thus isotherms in only one region need be considered. The problem has an analytic solution with which the results of the IMM agree well, as the authors showed.

Our extension of the IMM can be used only with boundary condition (Eq. 7), i.e., constant surface temperature. For the radiation-type boundary condition of Eq. 6 we introduce in Section V the Modified Isotherm Migration Method (MIMM). In both cases we need to know the temperature at the midplane to be able to move the isotherm closest to $X = 1$. This temperature at $X = 1$ is evaluated by extrapolation: a parabola is constructed such that it passes through (X_{m-1}^n, u_{m-1}^n) and (X_m, u_m) and has its maximum at $X = 1$, so that boundary condition (Eq. 4) is satisfied. Now the derivatives in Eq. 16 or 17 have to be approximated by uncentered finite differences:

$$X_m^{n+1} = X_m + 2\gamma\Delta T\frac{(pq^2 + qp^2)\,[q - (q + p)X_m + pX_{m-1}]}{[q^2 - (q^2 - p^2)X_m - p^2X_{m-1}]^2} \tag{31}$$

where

$$p \equiv u(1, T) - u_m, \quad q \equiv u_m - u_{m-1} \tag{32}$$

Similarly to Eqs. 28-30, Eq. 31 imposes a stability limit on ΔT:

$$\Delta T < \frac{[q^2 - (q^2 - p^2)X_m - p^2X_{m-1}]^2}{2\gamma(q + p)\,(pq^2 + qp)} \tag{33}$$

This too must be taken into account when we search for the lowest upper limit on ΔT^n. Equations 31 and 33 are written for the case where region 3 is adjacent to $X = 1$; when region 2 is adjacent to $X = 1$, we simply replace γ by α. Although in theory an isotherm cannot cross the midplane at $X = 1$, the isotherm immediately adjacent will do that because of our approximation. Once it passes $X = 1 - \epsilon_o$, ϵ_o being a small positive number which we usually take to be 0.001, the last isotherm is dropped and the next to the last isotherm takes its place as the last isotherm and is advanced by Eq. 31.

One set of problems that can be solved by the IMM is the heating or cooling of a one-component liquid initially at temperature u_o (which is not necessarily the transition temperature when the temperature) at $X = 0$ is changed abruptly and held at a constant temperature u_a. For a one-component liquid there are only two regions: liquid and solid. Analytic solutions are available for such problems in semi-infinite regions (e.g., Carslaw and Jaeger, 1959) be used for the initialization of the solution as long as the cooling (or heating) has not penetrated

appreciably toward $X = 1$; this we arbitrarily take as that period of time in which

$$\theta \equiv \frac{u(1, T) - u_a}{u_o - u_a} < 0.99 \tag{34}$$

The initial profile for the numerical solution is then given by

$$u_1 = u_a + \frac{(u_f - u_a)}{erf\lambda} erf\left(\frac{X}{2\sqrt{T}}\right) \quad \text{in region 1} \tag{35}$$

$$u_2 = u_o - \frac{(u_o - u_f)}{erfc(\lambda/\sqrt{\alpha})} erfc\left(\frac{X}{2\sqrt{\alpha T}}\right) \quad \text{in region 2} \tag{36}$$

where λ is calculated by

$$\frac{e^{-\lambda^2}}{erf\lambda} - \frac{\beta}{\sqrt{\alpha}} \frac{(u_0 - u_f)e^{-\lambda^2/\alpha}}{(u_f - u_a)erfc(\lambda/\sqrt{\alpha})} = \frac{\lambda S\sqrt{\pi}}{u_f - u_a} \tag{37}$$

and the position of the moving front is given by

$$X_f = 2\lambda\sqrt{T} \tag{38}$$

(X_f refers to the only front we have in this case.) The solution is initiated by choosing a T such that $\theta < 0.99$, determining the locations of the chosen isotherms in regions 1 and 2, and proceeding with the finite-difference scheme described above. In this case, only Eqs. 23, 24 and 27 are used for the single-phase transition front. It is important to note that the use of the analytic solutions, Eqs. 35-38, for various numerical initialization is merely a convenience and not a limitation to the method. Any techniques can be used to compute the temperature profile until the first moving front penetrates the sample, after which IMM can be applied.

The analytic solution for two moving fronts in a semi-infinite region is available (Carslaw and Jaeger, 1959), and can be used to start the solution in cases of finite slabs at constant initial temperature. Moreover, the solution for two fronts can be extended to three and more fronts. Again, the analytic solution is valid as long as Eq. 34 holds. The equations for the temperature in the three regions are:

$$u_1 = u_a + \frac{(u_{f1} - u_a)}{erf\lambda_1} \cdot erf\left(\frac{X}{2\sqrt{T}}\right) \tag{39}$$

$$u_2 = u_a + \frac{(u_{f2} - u_{f1})erf\left(\frac{X}{2\sqrt{\alpha T}}\right) + (u_{f1} - u_a)erf\lambda_2 - (u_{f2} - u_a)erf(\lambda_1/\sqrt{\alpha})}{erf\lambda_2 - erf(\lambda_1/\sqrt{\alpha})} \tag{40}$$

$$u_3 = u_0 - \frac{(u_0 - u_{f2})erfc\left(\frac{X}{2\sqrt{\alpha T}}\right)}{erfc(\lambda_2\sqrt{\alpha/\gamma})} \tag{41}$$

λ_1 and λ_2 are calculated by the simultaneous solution of two equations:

$$\frac{e^{-\lambda_1^2}}{erf\lambda_1} - \frac{(u_{f2} - u_{f1})\beta e^{-\lambda_1^2/\alpha}}{(u_{f1} - u_a)\sqrt{\alpha}[erf\lambda_2 - erf(\lambda_1/\sqrt{\alpha})]} - \frac{S_1\sqrt{\pi}\lambda_1}{u_{f1} - u_a} = 0 \tag{42}$$

$$\frac{e^{-\lambda_2^2}}{erf\lambda_2 - erf(\lambda_1/\sqrt{\alpha})} - \frac{(u_0 - u_{f2})}{(u_{f2} - u_{f1})} \cdot \delta\sqrt{\frac{\alpha}{\gamma}} \frac{e^{-\lambda_2^2\alpha/\gamma}}{erf(\lambda_2\sqrt{\alpha/\gamma})} - \frac{S_1\sqrt{\pi}\lambda_2}{u_{f2} - u_{f1}} = 0 \tag{43}$$

The positions of the two moving fronts are given by:

$$X_{f1} = 2\lambda_1\sqrt{T} \tag{44}$$

$$X_{f2} = 2\lambda_2\sqrt{\alpha T} \tag{45}$$

A value of T is chosen such that Eq. 34 is satisfied, the locations of the desired isotherms are determined from Eqs. 39-41, 44, and 45, and this initial profile is used to start the finite difference scheme.

All the isotherms that are to be used in the calculation are placed in the slab by the analytic solution; they span the entire temperature range $u_a \le u \le u_o$ and include, of course, the one or more transition fronts. Thus from the beginning of the numerical solution all the regions are present. The number of isotherms we choose in each region determines Δu. The spacings $X_{i+1} - X_{i-1}$ determine the maximum time step ΔT^n that ensures stability of the solution.

If the temperature at $X = 0$ were not constant, new isotherms would have to be introduced at $X = 0$ as the slab temperature changes. Now this is actually the case when there is thermal resistance at the surface and a radiation boundary condition is appropriate. The IMM cannot solve this kind of problem and a modification to it is needed. Addition of new isotherms is useful also when more accuracy is needed at a certain stage of the solution, e.g., near $X = 1$ as a moving front approaches and extrapolation to find the temperature at $X = 1$ becomes inaccurate because of the discontinuity of the first derivative of temperature at the moving front.

THE MODIFIED ISOTHERM MIGRATION METHOD (MIMM)

This modification is developed for a numerical solution of the problem of multiple phase transition fronts in a composite finite slab, with a radiation-type boundary condition (Eq. 13) at $X = 0$.

In each iteration of the MIMM the temperature at $X = 0$ is found; a new temperature difference, Δu_j, in the region j, the region between u_{fj} and $X = 0$, is calculated; new isotherms are assigned according to this Δu_j and located by interpolation between the old isotherms. Since we used finite differences approximations we interpolate here linearly, although parabolic or even a spline interpolation could be used. Figure 2 illustrates this procedure; the dashed lines denote the position of the isotherms of the n-th iteration and the dotted lines denote the new isotherms, while u_i and u'_i denote the temperatures of the old and the new isotherms. From the continuity of the heat flux at $X = 0$ we have

$$\frac{u_1 - u'_1}{X_1} = H_j(u'_1 - u_a), \tag{46}$$

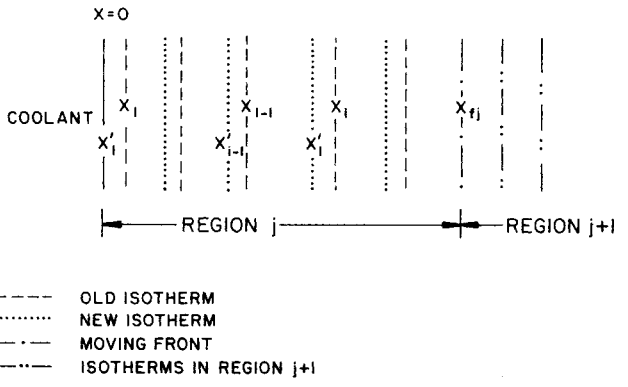

Figure 2. Reassignment of isotherms in the MIMM. X_i denotes the i-th isotherm in the n-th step; u_i is the temperature of this isotherm. For the $n+1$-th step new isotherms X'_i of temperature u'_i are located between the X_i isotherms.

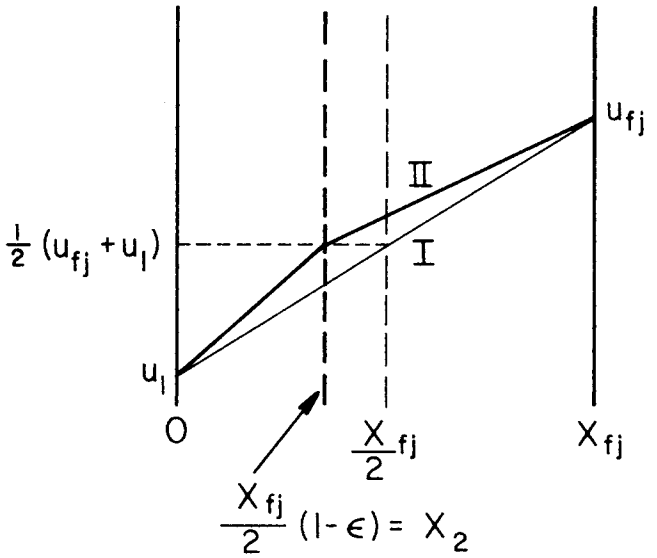

Figure 3. Placing the third isotherm between the moving front and $X = 0$. The temperature of the added (third) isotherm is the average of the temperature of its neighbors to the right and to the left; its position is left of the center-line between the moving front and $X = 0$. *I* is a linear profile while *II* is the profile after introduction of the third isotherm.

where H_j is a dimensionless heat transfer coefficient given by

$$H_j \equiv \frac{ah}{K_j}. \tag{47}$$

From Eq. 46 we get the new temperature at $X = 0$:

$$u_1' = \frac{u_1 + X_1 H_j u_a}{1 + X_1 H}. \tag{48}$$

The new temperature difference between the isotherms in region j is

$$\Delta u_j^{n+1} = (u_{fj} - u_1')/(N_j - 1). \tag{49}$$

N_j is the number of isotherms in region j. To limit the truncation error, which is proportional to $(\Delta u)^2$, this number can be increased as the solution progresses so that Δu_j^{n+1} does not exceed a tolerable maximum value. Linear interpolation gives the positions of the new isotherms:

$$X_i' = X_i + \frac{(X_i - X_{i-1})(u_i' - u_{i-1})}{(u_i - u_{i-1})} \tag{50}$$

Note that $u_{fj}' = u_{fj}$ and $X_{fj}' = X_{fj}$. The isotherms in the other regions remain unchanged.

As in the IMM, ΔT^n is determined by Eqs. 28-30 and 33, and the isotherms are advanced by Eqs. 23-27 at all stages of the MIMM solution.

Until $u(0, T)$ cools down to the highest freezing point, i.e., until the *first* moving front penetrates the sample, an accurate initial temperature profile can be calculated for initialization from an appropriate analytic or numerical solution for a finite slab. Thereafter the solution must be continued numerically with the MIMM. If Eq. 34 is still satisfied when $u(0, T)$ reaches the highest freezing point, then the solution for the corresponding semi-infinite case can be used. For a semi-infinite slab at constant initial temperature and with constant physical parameters, an analytic solution exists for the case of a radiation boundary condition. This solution (Schneider, 1955) expressed in our dimensionless variables is:

$$\theta \equiv \frac{u - u_a}{u_o - u_a} = erf\left(\frac{X}{2\sqrt{\alpha T}}\right) + \exp(H_l X + H_l^2 \nu T) erfc\left(H_l\sqrt{\nu T} + \frac{X}{2\sqrt{\nu T}}\right). \tag{51}$$

TABLE 1. THE EFFECT OF CHANGING I AND ϵ ON THE RESULTS OF MIMM CALCULATION FOR 1:1 TETRADECANE IN WATER DISPERSION. I IS THE NUMBER OF ITERATIONS THE FRONTS ARE HELD AT $X = 0$, ϵ IS THE DEVIATION FROM LINEARITY AFTER INTRODUCING THE THIRD ISOTHERM

	1	2	3	4
I	25	25	100	100
ϵ	0.05	0.15	0.05	0.15
T_s	6.79	6.73	6.81	6.75
$u(0, T_s)$	−40.16	−40.16	−40.16	−40.16

Here $\nu \equiv \kappa_j/\kappa_1$, $H_l \equiv ah/K_l$ and l denotes the liquid region. θ is set equal to 0.99 and T is calculated by the Newton-Raphson method from Eq. 51. This T is then used to calculate the positions of the isotherms between u_{fj}, the highest freezing point, and u_o, the initial temperature, from Eq. 53, also by the Newton Raphson method.

When Eq. 34 is not satisfied as $u(0, T)$ reaches the highest freezing point the infinite series solution for the finite-slab problem corresponding to Eq. 51 can be used. This standard solution (e.g., Kreith, 1973) expressed in our dimensionless variables is:

$$\theta = 4\sum_{n=1}^{\infty} \frac{\sin\lambda_n \cos[\lambda_n(1 - X)]}{2\lambda_n + \sin(2\lambda_n)} e^{-\lambda_n^2 \nu T} \tag{52}$$

where the λ_n are found by solving the transcendental equation

$$\lambda_n \tan\lambda_n = H_l. \tag{53}$$

The initial temperature profile is calculated by the same procedure as described for Eq. 51.

When an initial profile cannot be conveniently calculated, one can simply guess, say, a steep exponential and accept it as an adequate initial profile if a test shows that changing it has no appreciable effect on any quantity of interest, such as the time it takes to solidify completely the sample. As we show below, we have to do this in one of the later steps of the MIMM solution.

After the initial temperature has been determined, the problem remains of starting the movement of the phase-change front. The onset of a phase-change amounts to the introduction of a plane heat source (or sink), and the temperature profile in the slab must first adjust itself before the phase-change front can actually advance. To allow for the adjustment, the temperature at $X = 0$ is kept fixed at u_{fj} for I time steps. If the front is allowed to move before a certain critical number of iterations, it is found to move backwards. I should be chosen as small as possible, but we found that even if I was taken to be four times larger than the minimum requirement, the effect on T_s, the time for complete solidification, and on $u(0, T_s)$, the temperature at $X = 0$ at that time, was negligible, as shown by Table 1, which lists T_s and $u(0, T_s)$ as functions of I and ϵ (another parameter introduced below) when all other data are kept constant.

After I time steps the front u_{fj} is advanced according to an equation similar to Eq. 26 which accounts for the temperature gradients and thermal conductivities on both sides of the front. In the next time step the new temperature at $X = 0$ is calculated from the continuity of the heat flux at $X = 0$:

$$u_1 \equiv u(0, T) = (u_{fj} + u_a H_j X_{fj})/(1 + H_j X_{fj}). \tag{54}$$

This temperature is used to move u_{fj} in the next step.

When $u_{fj} - u_1$ exceeds the maximum temperature difference that we allow between isotherms in order to limit the truncation error of our calculation, a third isotherm must be added. By adding isotherms we also decrease the isotherm spacings and thus reduce the maximum time-step, which further reduces truncation error. Were a linear interpolation between the two isotherms ($u(0, T)$ and u_{fj}) to be used, the profile there would be linear and propagation would cease (a steady-state situation). Because we know from the earlier problems and from the initial profile that the profile is really not far from being linear, we can

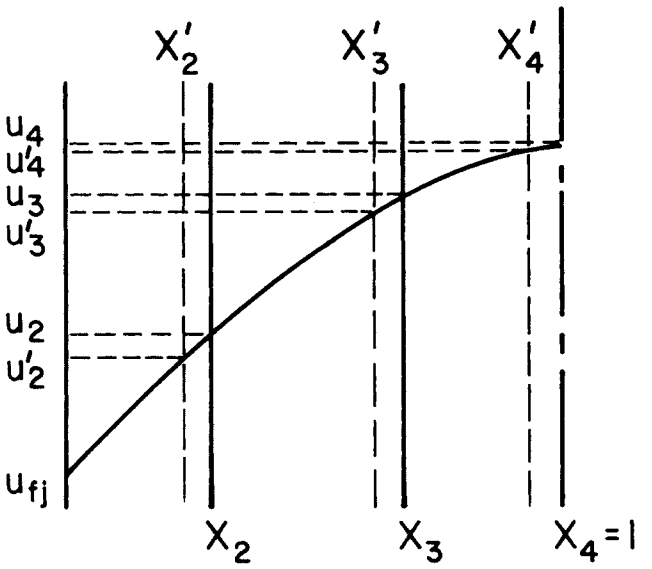

Figure 4. Addition of a fourth isotherm in the region near $X = 1$ when the number of isotherms in that region drops to three. X_i and u_i are the position and temperature of the isotherms before the addition; X'_i and u'_i are the position and temperature of the isotherms after the addition.

introduce a small deviation from linearity by assigning to the third isotherm a temperature

$$u_2 = \tfrac{1}{2}(u_{fj} + u_1) \tag{55}$$

and position

$$X_2 = \tfrac{1}{2}X_{fj}(1 - \epsilon) \tag{56}$$

where ϵ is a small positive number, Figure 3. For the initial profile calculated by the analytic solution, ϵ is between 0.04-0.06. Table 1 shows that changing ϵ from 0.05 to 0.15 has a negligible effect on T_s and $u(0, T_s)$. Once three isotherms are present the solution can proceed as described earlier.

Another feature of the MIMM is the addition of isotherms near $X = 1$ when u_{fj} approaches the midplane. Whenever the number of isotherms between u_{fj} and $X = 1$ falls below four (including u_{fj} itself), an isotherm is added; a new Δu_j in this region is calculated from

$$\Delta u_j = [u(1, T) - u_{fj}]/4, \tag{57}$$

and four new isotherms are located in this region. The first coincides with u_{fj}, the second and third are placed by linear interpolation between the old isotherms, and the fourth is placed by fitting a parabola through the old third and fourth isotherms, the latter being now at $X = 1$, such that the parabola has its maximum at $X = 1$. The temperature of the new fourth isotherm is on this parabola as Figure 4 shows. As the solution proceeds the region between u_{fj} and X_j becomes smaller and smaller and the temperature profile in this region becomes flatter, until for all practical purposes it is flat. From that stage the solution is continued by assuming that the temperature is uniform in the region closest to $X = 1$.

NUMERICAL RESULTS

For the purpose of comparison we first give results for a case in which there is no thermal resistance at the interface between a freezing slab of water and a liquid cryogen, an unrealistic situation that can nevertheless give us an idea of the upper limit of cooling rates if no external thermal resistances exist. Figure 5 shows the temperature profiles calculated for freezing water initially at 20°C by suddenly exposing the surface at $X = 0$ to a coolant at −150°C, as in methods of rapidly solidifying thin liquid specimens for cold-stage electron microscopy. Only Eqs. 25, 26 and 28 were used for the single phase-transition front. Data used were: $\kappa_{water} = 1.44 \times 10^{-7}$ m²/s, $K_{water} = 55.2$ W/m°K, $\alpha = 0.125$, $\beta = 0.272$, $S = 160$°K. In Figure 5, 1 denotes the solid region below 0°C and 2 denotes the liquid region above 0°C. The time to complete solidification of water was 0.809 dimensionless time units; for a 200 nm thick sample of water this corresponds to 7.03×10^{-9} seconds or an average cooling rate of 2.84×10^{9}°C/s; for a 20 mm thick sample, the freezing time is 70.3 seconds with an average cooling rate of 0.284°C/s.

The IMM was also used to solve the problem of two fronts moving through a freezing dispersion of tetradecane in water. As in the previous case, we assumed negligible resistance to heat transfer at the slab-coolant interface. Tetradecane freezes at 6°C and water at 0°C; we need the thermal diffusivities and thermal conductivities of the three regions formed by the two freezing fronts. We evaluate these properties in each region from the properties of the pure components by the method suggested by Jefferson et al. (1958) for dispersions and suspensions. Let ϕ be the volume fraction of the dispersed phase, K_d its thermal conductivity and K_c the thermal conductivity of the continuous phase. We define a geometrical parameter

$$\psi = 0.403\phi - 0.500, \tag{58}$$

and introduce

$$K' \equiv \frac{2K_cK_d}{K_d - K_c}\left[\frac{K_d}{K_d - K_c}\ln\left(\frac{K_d}{K_c}\right) - 1\right] \tag{59}$$

The effective thermal conductivity of the region is given by

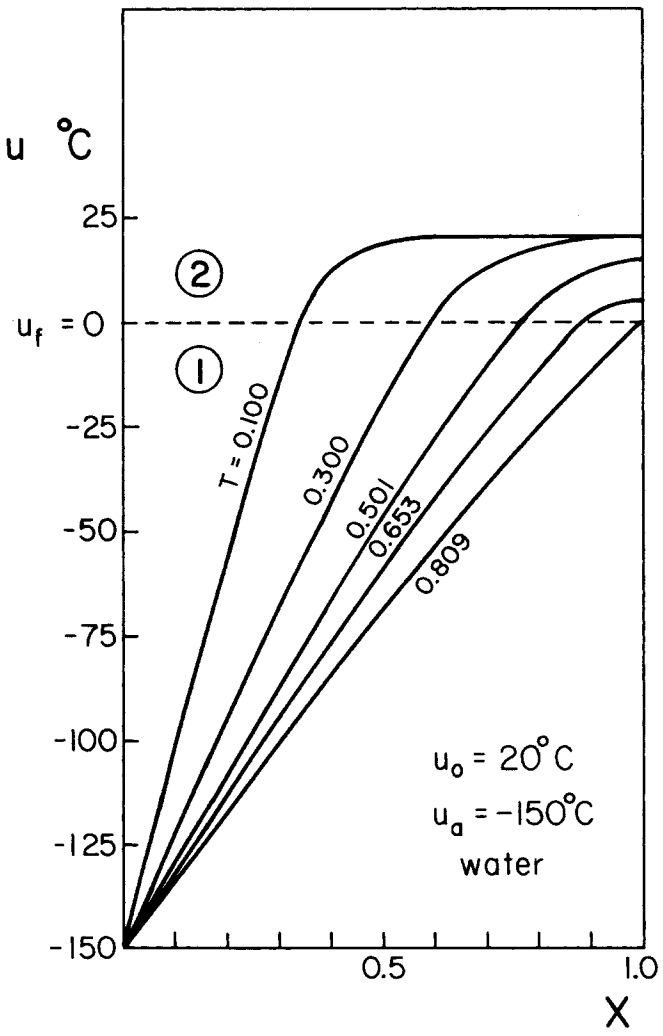

Figure 5. Temperature profiles in a slab of water at different times during freezing. No resistance at $X = 0$. ① is the solid region; ② is the liquid region. IMM was used.

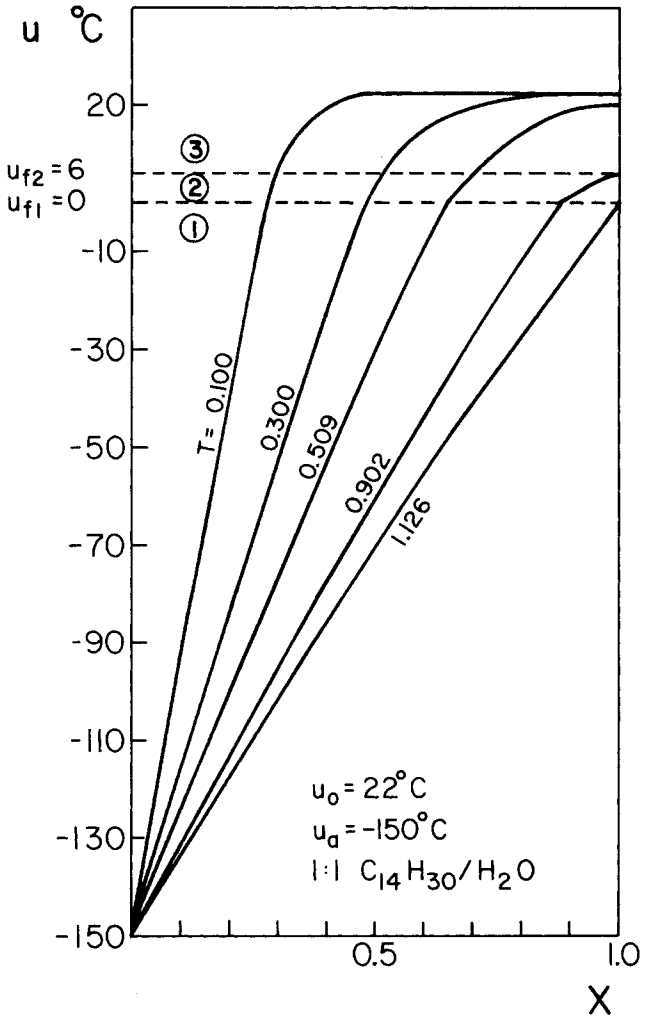

Figure 6. Temperature profiles in a freezing slab of 1:1 tetradecane/water dispersion calculated with IMM. ① is the solid-solid region, ② is the solid-liquid region and ③ is the liquid-liquid region. No resistance at X = 0.

$$K_{eff} = K_c \frac{(1 + 2\psi)^2 - \pi/4}{(1 + 2\psi)^2} + \frac{\pi}{4(1 + 2\psi)^2}\left[\frac{(\psi + 0.5)K'K_c}{0.5K_c + \psi K'}\right] \tag{60}$$

Thermal capacities were calculated by assuming additivity of the thermal capacities of the two phases. The density of the dispersion was calculated in the same way. Jefferson et al. (1958) found experimentally that their method for calculating the effective thermal conductivity holds for dispersed and continuous phases thermal conductivities of which differ by a factor of 10. Thus, we found no need to use more sophisticated methods for calculating K_{eff}.

Figure 6 shows temperature profiles calculated using IMM for freezing a dispersion of tetradecane in water with boundary Eq. 7 (i.e., $h \to \infty$). Water is the continuous phase with volume fraction of 0.5. Values of parameters for this system are given in Table 2. The corresponding reduced parameters are $\alpha = 0.261$, $\beta = 0.446$, $\gamma = 0.119$, $\delta = 0.465$, $S_1 = 233°K$, $S_2 = 53.4°K$. The temperature of the coolant is −150°C; the initial temperature 22°C. In Figure 6 we notice three regions: 1—solid-solid below 0°C, 2—solid-liquid—between 0°C and 6°C, and 3—liquid-liquid—above 6°C. Complete solidification is achieved in 1.13 dimensionless time units; for a 200 nm thick sample of 1:1 tetradecane/water dispersion this corresponds to 1.25×10^{-9} seconds—an average cooling rate of 1.76×10^{9}°C/s. The time step ΔT varied from 5.08×10^{-5} at the start of the calculation to 2.95×10^{-3} at the end, when the isotherms were further apart.

As a one-phase example of application of the MIMM, we considered a slab of water with a Biot number, $Bi \equiv ha/K_w$, equal to 0.95. This is an intermediate value for which neither boundary Eq. 7 nor the Newtonian cooling approximation is valid. The slab is initially at 22°C and the coolant is at −150°C. In this calculation we took $I = 50$ and $\epsilon = 0.05$. Temperature profiles are shown in Figure 7. 1 denotes the solid region below

TABLE 2. DATA USED FOR THE COMPUTATIONS OF SOLIDIFICATION OF A 1:1 TETRADECANE-WATER DISPERSION

Region	$K \times 10^3$ °K/m² °K	$\kappa \times 10^7$ m²/s	$\rho \times 10^{-3}$ kg/m³	c kJ/kg °K
1	14.4	9.00	0.846	1.90
2	64.4	2.35	0.887	3.08
3	29.9	1.07	0.882	3.18

Volume fraction of water = 0.5.
Heat of fusion of water = 334 kJ/kg.
Heat of fusion of tetradecane = 224 kJ/kg.

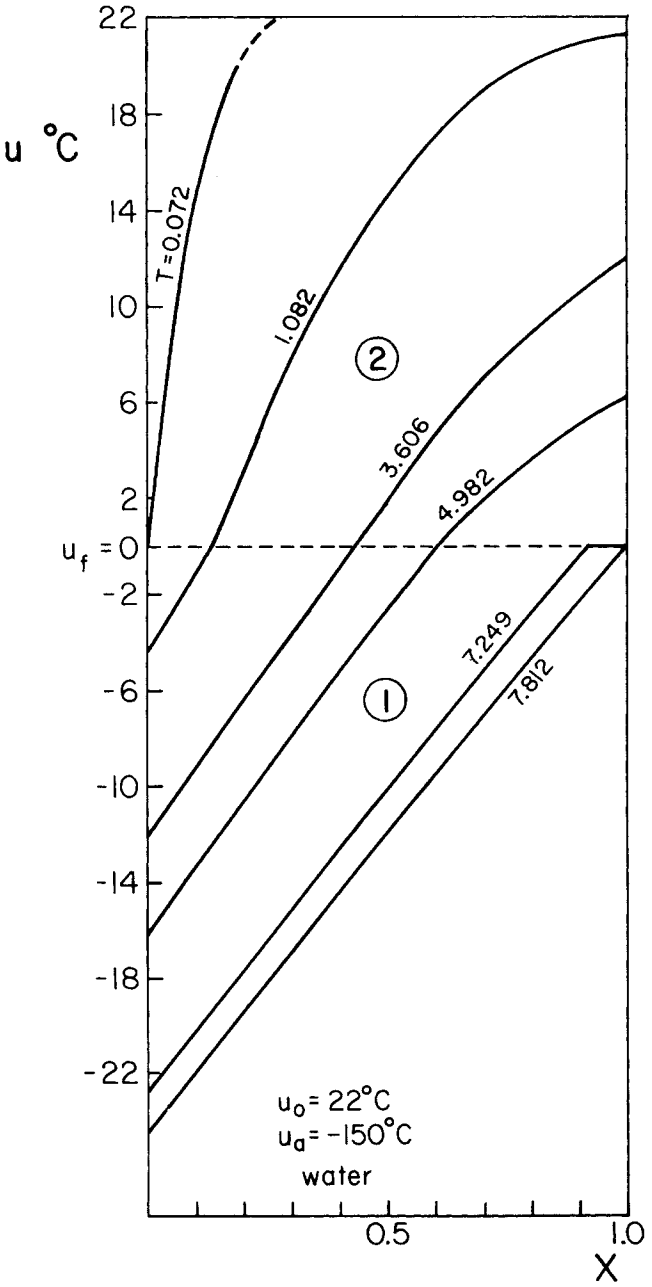

Figure 7. Temperature profiles in a freezing slab of water calculated with the MIMM. Bi ≡ ha/K_w = 0.95.

0°C and 2 denotes the liquid region above 0°C. Note that the temperature profile at $T = 7.249$ is practically flat at 0°C in the liquid region. Complete solidification occurred after 7.812 dimensionless time units; for a water sample 200 nm thick the time to achieve complete solidification is 6.30×10^{-8} seconds. The average cooling rate is 3.49×10^{8}°C/s. For a 20 mm sample the freezing time is 630 seconds. When complete solidification is achieved the temperature at $X = 0$ is −24.5°C.

Figure 8 shows the temperature profiles obtained by applying MIMM to 50% (by volume) tetradecane dispersed in water. The coolant here is also at −150°C, the initial slab temperature at 22°C, and the Biot number ($Bi \equiv ha/K_3$) is 1.75. Each front was held for 25 steps when it appeared at $X = 0$ ($I = 25$); this corresponds to 6.76×10^{-3} dimensionless time units for the 6°C front and to 2.27×10^{-3} units for the 0°C front. We took $\epsilon = 0.05$ for the introduction of the third isotherm in both cases. The time for complete solidification is 6.79; for a 200 nm sample the corresponding real time is 7.54×10^{-8} seconds and the average cooling rate is 2.92×10^{8}°C/s. Table 1 shows the effect of changing I and ϵ on T_s and $u(0, T_s)$. When complete solidification of the sample occurred the temperature at $X = 0$ was −40.2°C. The three regions in Figure 8 are marked in the same way as the regions in Figure 6.

We obtained, but do not present here, temperature profiles for the 1:1 tetradecane/water slab for Biot numbers ranging from 0.058 to 15. For Bi = 15 the profiles are quite close to those of Figure 6 (the case of $Bi \to \infty$). For Bi = 0.058, the smallest Biot number considered, the results are similar but not identical to those computed from the Newtonian cooling model (infinite thermal conductivities of the slab materials)—the freezing time estimated by the Newtonian cooling model is 32% too low for the case of Bi = 0.058.

DISCUSSION

These numerical results demonstrate the utility and flexibility of our version of the Isotherm Migration Method and the new Modified Isotherm Migration Method. The former can be used to solve the multi-component, one-dimensional Stefan problem with any given initial temperature profile, where one or more moving phase-transition fronts are present and the surface temperature is constant.

In practical situations where the goal is to produce a very rapid transformation in the entire slab (and even more so when the goal pertains only to some portion of it near its surface), surface and external resistances often turn out to be controlling, and so one needs a method that can handle varying surface temperature. The MIMM can, as demonstrated above, be used to solve the one-dimensional Stefan problem for multifront propagation in a slab subject to a radiation-type boundary condition.

The numerical methods we have used can also uncover ranges of conditions and parameters in which reasonably accurate approximations can be made that reduce effort and computational cost. We demonstrate this for the case of the 1:1 tetradecane/water freezing problem that was discussed in the previous section.

Table 3. Reduced Freezing Times, T_s, and Final Surface Temperatures $u(0, T_s)$, Predicted for the 1:1 Tetradecane-Water Dispersion for Various Biot Numbers ($B_i \equiv ha/K_3$)

B_i	T_s	$u(0, T_s)$ °C
∞	1.13	−150
15.0	2.07	−119.8
7.0	2.66	− 91.4
3.5	4.06	− 62.8
1.75	6.79	− 40.2
0.87	12.44	− 23.5
0.58	17.80	− 16.7
0.058	167.20	− 1.8

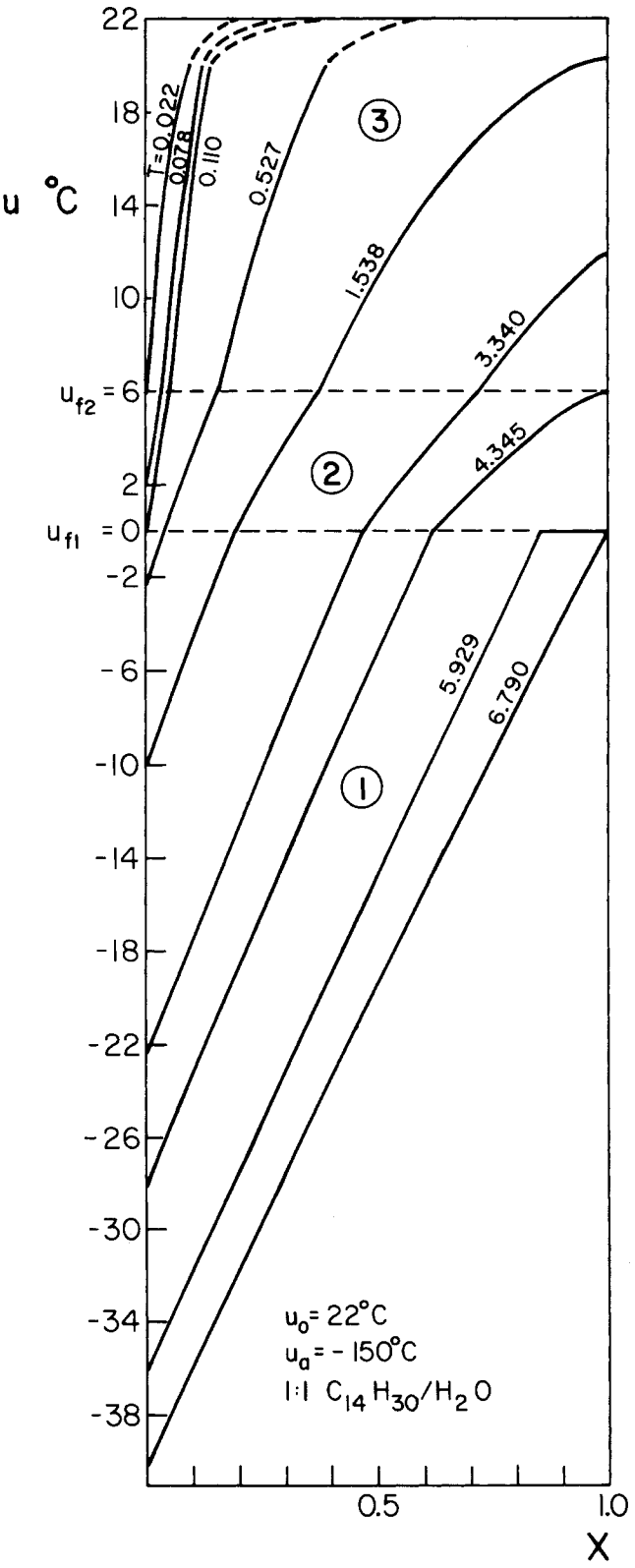

Figure 8. Temperature profiles in a freezing slab of 1:1 tetradecane/water dispersion calculated with the MIMM. Bi ≡ ha/K_3 = 1.75.

The reduced freezing time (the time it takes for both phases to freeze throughout the slab), T_s, and the surface temperature reached at that time, $u(0, T_s)$, are summarized in Table 3 for the Biot numbers we considered. For Biot numbers lying between 0.058 and 7 the freezing time obeys the linear relationship

$$T_s = 9.67\ \mathrm{Bi}^{-1} + 1.27 \tag{61}$$

Even for higher Biot numbers the formula is quite good, with less than 1% error. At Bi = 15 it predicts $T_s = 1.91$ vs. the computed value 2.07; in the limit as Bi $\to \infty$ it predicts 1.27 vs. the computed value 1.13.

The simple relation (Eq. 61) results because the frontal propagation controls the heat transfer rate in the hydrocarbon-water system considered here. That such is the case can be construed from a simple model. In the Newtonian cooling limit (Kreith, 1973) we find that the time to cool the sample to the temperature at which the first freezing front enters is only about 10% of the time T_s. And from the temperature profiles computed by the MIMM, we see that the temperature varies almost linearly within each region of the freezing slab. If we ignore the temperature gradient between the center of the slab and the nearest freezing front, i.e., if we neglect sensible heat transfer in this region, and assume linear temperature profiles in the other regions, the equation of frontal propagation is

$$(1 - \phi)\rho_h l_h \frac{dx_{f2}}{dt} = \frac{u_{f2} - u_a}{h^{-1} + x_{f2}K_2^{-1}} \tag{62}$$

when only the hydrocarbon freezing front is in the slab. l_h, ρ_h are the latent heat of freezing and the density of the hydrocarbon. When the hydrocarbon and water fronts are both in the slab, the corresponding equations are

$$\phi\rho_w l_w \frac{dx_{f1}}{dt} = \frac{u_{f1} - u_a}{h^{-1} + x_{f1}K_1^{-1}} - \frac{K_2(u_{f2} - u_{f1})}{x_{f2} - x_{f1}} \tag{63}$$

and

$$(1 - \phi)\rho_h l_h \frac{dx_{f2}}{dt} = \frac{K_2(u_{f2} - u_{f1})}{x_{f2} - x_{f1}} \tag{64}$$

l_w, ρ_w are the latent heat and the density of freezing of the water.

Equation 62 can be integrated between $t = 0$ and t_s, the time for surface temperature to reach u_{f1}. The result is

$$t_1 = \frac{(1 - \phi)\rho_h l_h b}{u_{f2} - u_a}\left(h^{-1} + \frac{b}{2}K_2^{-1}\right) \tag{65}$$

where $b = x_{f2}(t_1)$. Adding Eqs. 63 and 64, multiplying the result by $h^{-1} + x_{f1}K_1^{-1}$, and integrating, we obtain

$$\phi\rho_w l_w a\left(h^{-1} + \frac{a}{2}K_1^{-1}\right) + (1 - \phi)\rho_h l_h \int_b^a (h^{-1} + x_{f1}K_1^{-1})dx_{f2} = (u_{f1} - u_a)t_2 \tag{66}$$

If the freezing time is estimated as $t_1 + t_2$, then Eqs. 65 and 66 yield for the water-hydrocarbon dispersion of interest here

$$T_s = \frac{\kappa_1}{a^2}(t_1 + t_2) = (8.26 - 0.030b/a)\ \mathrm{Bi}^{-1} + [0.777 + 0.159d + 0.171(b/a)^2] \tag{67}$$

where

$$d \equiv \frac{1}{a^2}\int_b^a x_{f1}dx_{f2}. \tag{68}$$

At one extreme $b = 0$ and $d = 0.5$, and at the other extreme $b = a$ and $d = 0$. Correspondingly

$$T_s = 8.26\ \mathrm{Bi}^{-1} + 0.857, \quad b = 0, \quad d = 0.5 \tag{69}$$

and

$$T_s = 8.23\ \mathrm{Bi}^{-1} + 0.948, \quad b = a, \quad d = 0 \tag{70}$$

Thus over the range of values possible for b and d, the slope of T_s vs. Bi^{-1} is almost constant. The intercept varies somewhat more, but not widely. Equation 67 underestimates (by approximately 15%) the actual freezing time. This is consistent with the simple model on which Eq. 67 is based. The agreement between the simple model and the linear fit support our claim that the linear fit works because frontal propagation controls the rate of heat transfer in the case considered.

The IMM and its modifications can be used to solve a variety of one-dimensional Stefan problems with any number of moving fronts and any range of parameters. The key to applying the IMM is the appropriate management of isotherms according to the specific parameters of the problem—starting with a number of isotherms with suitable intervals and then eliminating them one by one as the solution propagates, or starting with an initial profile and then adding and eliminating isotherms in order to limit the temperature differences to control truncation error.

We have illustrated application of the IMM and MIMM to problems of freezing a dispersion. But the method can be used for any other one-dimensional problem that involves moving fronts of phase-transition with either a fixed surface temperature or with a radiation-type boundary condition. The basic Isotherm Migration Method was extended by Crank and Gupta (1975) to two-dimensional problems; we are now in the process of extending our Modified Isotherm Migration Method to two-dimensional cases.

ACKNOWLEDGMENT

This research was supported by the National Science Foundation and the Department of Energy in connection with basic studies directed toward enhancing petroleum recovery.

NOTATION

a = half width of the slab, m
Bi = Biot number, $ha/°K$
b = $x_{f2}(t_1)$, position of front no. 2 when surface temperature reached is that of front no. 1
d = defined by Eq. 68
H_j = dimensionless heat transfer coefficient, ah/K_j (≡ Biot number)
h = heat transfer coefficient, J m^{-1} s^{-1} °K^{-1}
I = number of iterations a moving front is held at $X = 0$
K = thermal conductivity, J m^{-2} s^{-1} K^{-1}
L = $l\phi$, J kg^{-1}
l = latent heat of phase change, J kg^{-1}
N_j = number of isotherms in region j
p = temperature difference defined by Eq. 32, °K
q = temperature difference defined by Eq. 32, °K
S = reduced latent heat of change of phase, °K
T = dimensionless time, a^2t/κ_1
t = time, s
u = temperature, °C
X = dimensionless distance, x/a
x = distance, m

Greek Letters

α = κ_2/κ_1
β = K_2/K_1
γ = κ_3/κ_1
ΔT = dimensionless time step
Δu_i = temperature difference between isotherms, °K
δ = K_3/K_2
ϵ = deviation from linearity, Eq. 56
ϵ_n = distance from $X = 1$ at which isotherms are eliminated
θ = dimensionless temperature, $(u - u_a)/(u_o - u_a)$
κ = thermal diffusivity, m^2 s^{-1}
λ_1, λ_2 = coefficients in Eqs. 44, 45
λ_n = eigenvalues given by Eq. 53
ν = κ_j/κ_1
ρ = density, kg m^{-3}
ϕ = volume fraction
ψ = geometrical parameter given by Eq. 58

Subscripts

a = ambient
f = moving front
$f1$ = moving front no. 1
$f2$ = moving front no. 2
fi = i-th moving front
fj = moving front closest to $X = 0$
h = hydrocarbon
i = region i or i-th isotherm
j = region j or in the region closest to $X = 0$
l = liquid
m = isotherm closest to $X = 1$
o = initial temperature
s = at complete solidification
w = water

Superscripts

n = n-th time step

LITERATURE CITED

Carslaw, H. S., and J. C. Jaeger, "Conduction of Heat in Solids," Chap. XI, Clarendon Press, Oxford (1959).

Chernous'ko, F. L., "Solution of Non-Linear Heat Conduction Problems in Media with Phase Change," *Int. Chem. Eng.*, **10**, 42 (1970).

Crank, J., and R. D. Pahle, "Melting Ice by Isotherm Migration Method," *Bull. J. Inst. Maths. Applics.*, **9**, 12 (1973).

Crank, J., and R. S. Gupta, "Isotherm Migration Method in Two Dimensions," *Int. J. Heat Mass Transfer*, **18**, 1101 (1975).

Dix, R. C., and J. Cizek, "The Isotherm Migration Method for Transient Heat Conduction Analysis," Proc. Fourth Int'l Heat Transfer Conference, Paris, **1**, ASME New York (1971).

Jefferson, T. B., O. W. Witzell and W. L. Sibit, "Thermal Conductivity of Graphite-Silicone Oil and Graphite-Water Suspensions," *Ind. Eng. Chem.*, **50**, 1589 (1958).

Kreith, F., *Principles of Heat Transfer*, 3rd ed. IEP, New York (1973).

Schneider, P. J., *Conduction Heat Transfer*, Addison-Wesley, Cambridge, MA (1955).

Shamsundar, N., "Comparison of Numerical Methods for Diffusion Problems with Moving Boundaries," *Moving Boundary Problems*, D. G. Wilson, A. D. Solomon, and P. T. Boggs, eds., p. 165, Academic Press, New York (1978).

Manuscript received July 25, 1980; revision received December 8, and accepted January 20, 1981.

Modeling of Three Phase Reactors: A Case of Oxydesulfurization of Coal

J. B. JOSHI

J. S. ABICHANDANI

and

Y. T. SHAH

Department of Chemical and Petroleum Engineering
University of Pittsburgh
Pittsburgh, PA

and

J. A. RUETHER

and

H. J. RITZ

Pittsburgh Energy Technology Center
U.S. Department of Energy
Pittsburgh, PA 15213

Mathematical models have been developed for the design of bubble column slurry reactors, wherein the solids take part in the reaction and follow the shrinking core model. The cases of liquid film control, ash diffusion control, and chemical reaction control have been analyzed. Experiments were performed in a 22.2 mm i.d. continuous cocurrent bubble column slurry reactor for the removal of pyritic sulfur by oxidation from aqueous slurries of Upper Freeport, Lower Freeport, Kentucky No. 9, and Pittsburgh seam coals, in the temperature range of 430-480°K at 6.8 MPa total pressure. The theoretical predictions are found to be in good agreement with experimental results.

SCOPE

Bubble column slurry reactors are very popular in industry situations where the solids either take part in the reaction or act as catalyst. In this investigation, solids that do not change particle size during the reaction are investigated. The performance of such reactors will depend upon interphase, inter- and intra-particle mass and heat transfer, and the intrinsic chemical kinetics. It is well known that backmixing is detrimental to the conversion. Using dispersion models, earlier studies have accounted for the extent of backmixing. However, for situations where solids take part in a reaction that is described by nonlinear rate equations, the dispersion models are not applicable and it is necessary to develop models based on the exit age distributions.

In an application of the models, experiments were performed on the removal of pyritic sulfur from coal by oxidation with air in a continuous bubble column slurry reactor. The effects of temperature, reaction time, and superficial gas velocity were investigated. Some scale-up considerations are examined.